Published in final edited form as:

Nat Microbiol. 2020 January ; 5(1): 76–83. doi:10.1038/s41564-019-0618-z.

Evolution of the innate and adaptive immune response in women with acute Zika virus infection

Pierre Tonnerre[1,*,§], **Juliana G Melgaço**[1,2,*], **Almudena Torres-Cornejo**[1], **Marcelo A Pinto**[2], **Constanze Yue**[3], **Johannes Blümel**[3], **Paulo Sergio Fonseca de Sousa**[2], **Vinicius da Motta de Mello**[2], **Julio Moran**[4], **Ana M Bispo de Filippis**[2], **David Wolski**[1], **Alba Grifoni**[5], **Alessandro Sette**[5,6], **Dan H Barouch**[7,8], **Ruben C Hoogeveen**[1], **Sally A Baylis**[3], **Georg M Lauer**[1,&,#], **Lia L Lewis-Ximenez**[2,&,#]

[1.]Division of Gastroenterology, Massachusetts General Hospital and Harvard Medical School, Boston, MA, USA. [2.]Oswaldo Cruz Institute, FIOCRUZ, Rio de Janeiro, Brazil. [3.]Division of Virology, Paul-Ehrlich-Institut, Langen, Germany. [4.]Dr. Julio Moran Laboratories, Herrliberg, Zurich, Switzerland. [5.]Division of Vaccine Discovery, La Jolla Institute for Immunology, La Jolla, CA, USA [6.]Department of Medicine, University of California San Diego, La Jolla, CA, USA. [7.]Ragon Institute of MGH, MIT and Harvard, Cambridge, MA, USA. [8.]Center for Virology and Vaccine Research, Beth Israel Deaconess Medical Center, Boston, MA, USA.

Zika virus (ZIKV) is a *Flavivirus* closely related to other human pathogens such as Dengue virus (DENV)[1]. Primary transmission usually involves *Aedes aegypti*, which has expanded its distribution range significantly[2], though rarer infection routes including mother-to-fetus transmission, sexual contact and blood transfusion have also been observed[3-7]. Primary ZIKV infection is usually asymptomatic or mild in adults, with quickly resolved blood viremia, but ZIKV might persist for months in saliva, urine, semen, breast milk and the central nervous system[8-12]. During a recent ZIKV outbreak in South America, significant numbers of neurological complications such as Guillain-Barré syndrome were reported[13,14], together with cases of microcephaly and associated developmental problems in infants born to women infected with ZIKV during pregnancy[15-20], raising the clinical significance of this

[#]To whom correspondence should be addressed: Georg M. Lauer, MD, PhD, glauer@mgh.harvard.edu; Lia L. Lewis-Ximenez. MD, PhD, lialewis.fiocruz@gmail.com.

Author contributions: P.T., J.G.M. and A.T.-C. conceived and designed the study. P.T., J.G.M., A.T.-C. and R.C.H. performed immunophenotyping and intracellular cytokine stainings by flow-cytometry. J.G.M., P.S.F.S., V.M.M., and L.L.L.X. collected clinical data and biological samples. C.Y., A.M.B.F., and S.A.B. performed ZIKV-RNA detection assays. J.G.M., C.Y., M.A.P, J.M. and S.A.B. performed anti-ZIKV antibody ELISA assays. C.Y. and J.B. performed ZIKV-neutralizing antibody assays. D.W., A.G., A.S., D.H.B., S.A.B., L.L.L.X. contributed to the study design and data interpretation. G.M.L. conceived and supervised the study, and provided funding. P.T. and G.M.L. analyzed the data and wrote the manuscript.

[*]Authors contributed equally

[§]Present address: Institut Pasteur, Biodiversity and Epidemiology of Bacterial Pathogens, Paris, France

[&]Authors contributed equally

Conflicts of interest: J.M. is the owner of Dr. Julio Moran Laboratories, a company owning and distributing for Research Use Only (RUO) the ELISA assays DIACHECK for the detection of anti-human ZIKV antibodies. The remaining authors declare no competing interests.

Data availability: The data that support the findings of this study are available from the corresponding authors upon request.

infection. Analyses of the human immune response to ZIKV are scarce[21-28], but the recent outbreak has provided an opportunity to assess ZIKV immunity using current immunological methods. Here, we comprehensively assessed the acute innate and adaptive immune response to ZIKV infection in ten female subjects recruited during early infection and followed through reconvalescence. We define a cascade of events leading to immunological control of ZIKV, with previous exposure to DENV impacting some, but not all mediators of antiviral immunity.

The ten women with confirmed and documented acute ZIKV infection were followed throughout infection at the Viral Hepatitis Ambulatory Clinic, Oswaldo Cruz Foundation, Rio de Janeiro, Brazil. All subjects tested positive for plasma and urine ZIKV RNA as well as for anti-ZIKV IgM and/or IgG antibodies. None of the patients presented with detectable IgM antibodies against DENV, but 6/10 tested positive for anti-DENV IgG confirming previous DENV exposure. One patient reported having received Yellow Fever virus (YFV) vaccine previously. Fig. 1a illustrates the detailed clinical course of a 31-year-old woman as a typical example of symptomatic ZIKV infection. The longitudinal specimens from this cohort were divided into three different timeframes post-infection: the acute phase (A, < 14 days), the recovery phase (R, between days 14 and 56), and the follow-up phase (FU, 56 to 224 days) (Fig. 1b). The presence and pattern of symptoms and plasma ZIKV-RNA detection during these phases are indicated in Fig. 1c. Patient demographics and HLA-types are available in Extended Data Table 1. Individual symptom occurrence and plasma ZIKV-RNA levels are detailed in Extended Data Fig. 1.

First, we monitored different innate sensor cell subsets of monocytes and dendritic cells, as well as myeloid-derived suppressor cells (MDSCs) (Extended Data Fig. 2a), as those cell types are key modulators of subsequent adaptive immune responses and can also be infected by ZIKV [29-32]. We observed an increase in the relative frequency of intermediate monocytes (CD16+CD14+) within the earliest phase of infection compared to follow-up time points in the same patients and healthy controls, mirrored by a decrease in classical monocytes (CD16-CD14+). We also observed a relative reduction in mDC populations with a profound shift toward a dominance of pDCs versus mDCs as early as the changes in monocyte populations (Fig. 1d and Extended Data Fig. 3a,b). Both intermediate monocytes and mDCs have been identified as possible compartments of ZIKV replication, but they seem to respond differently to infection, with either activation and expansion or conversely apoptotic cell death [29-31,33]. The observed early changes were temporary and both monocyte and DC compartments returned to normal distribution patterns observed in healthy controls by the end of the acute infection phase, consistent with other reports [26,29]. Intermediate monocytes produce large amounts of pro-inflammatory cytokines and possess high phagocytic potential, leading to the induction of plasmablast differentiation and T cell activation [34]. Thus, we also studied general activation of immune cells from the adaptive immune system, measuring the frequency of plasmablasts and activated CD8+ T cells over time (Extended Data Fig. 2b). Again, similar to the innate immune cells, we observed increased frequencies of plasmablasts as well as CD38high CD8+T cells at the earliest observation time points, with rapid normalization upon entry into reconvalescence (Fig. 1d and Extended Data Fig. 3c,d). That we observe not only a significant containment of ZIKV viremia contemporaneously with the increase in the intermediate monocyte population, but also plasmablast induction

and high activation levels of CD8+ T cells supports the idea that these monocytes with an intermediate phenotype play a key role in both ZIKV control and the induction of adaptive immunity [29]. Previous exposure to DENV did not affect these results. Together, the data indicate a rapid and broad immune activation with the onset of symptoms of ZIKV infection, followed by a rapid return to a general status similar to what is observed in healthy individuals.

Vaccine-induced protection from ZIKV infection is believed to be mediated, at least in part, by the induction of potent neutralizing antibodies [35,36], as suggested in experimental models of infection [37,38]. Given the limited data on the neutralizing antibody response in natural human infection, and the potential impact of previous exposure to other Flaviviruses, most notably DENV, we monitored the evolution of anti-ZIKV IgM, IgA, IgG and neutralizing antibodies in this cohort using ELISA assays based on a viral lysate containing structural as well as non-structural ZIKV proteins. Anti-ZIKV IgM were usually detectable early in the acute phase and declined thereafter (Fig. 2a). Anti-ZIKV IgA closely mirrored IgM responses (Fig. 2b), while IgGs developed later with maximum IgG levels coinciding with clinical recovery and persisting throughout the follow-up of up to 200 days (Fig. 2c). No manifest differences between DENV-naïve and DENV-experienced patients were observed for the kinetics of both IgA and IgM responses (Fig. 2a,b and Extended Data Fig. 4a). In contrast, previous exposure to DENV was associated with earlier detection and higher plasma levels of IgG, with positive titers at the earliest timepoints following symptom onset and no lag time after the detection of IgM and IgA responses (Fig. 2d), supporting the presence of DENV cross-reactive memory B cells rapidly responding to ZIKV infection [23,39], even though we did not observe a faster and greater expansion of plasmablasts, as suggested in a previous study describing antibody cross-reactivity [39] (Fig. 1d). Similar results were obtained with a different ELISA assay employing a single ZIKV-specific epitope niched in NS1 protein (Extended Data Fig. 4b,c). The emergence of antibodies with neutralizing capabilities paralleled the anti-ZIKV IgG response, with peak magnitude observed during the recovery phase and persistent neutralization throughout follow-up (Fig. 2e and Extended Data Fig. 5). Notably, plasma samples with the highest titers of neutralizing antibodies also had the highest IgG responses and were found in DENV-experienced patients, compared to DENV-naives (Fig. 2f). While our results identify distinct patterns in the dynamics and the intensity of anti-ZIKV IgG and neutralizing antibodies production between DENV-experienced and DENV naïve patients during acute and recovery phases of infection, the antibody responses become more similar for the parameters we measured once the virus was cleared, thus suggesting limited long-term differences. Whether DENV-specific pre-existing humoral responses are mainly an asset to ZIKV control, or whether they can also be detrimental through antibody-dependent enhancement (ADE) or lead to limited efficacy due to original antigenic sin remains unknown [40-44]. Resolving this question has clear relevance to the development of integrated vaccination strategies against *Flaviviruses* with shared endemic areas.

We then monitored ZIKV-specific CD4+ and CD8+ T cells in 6 ZIKV-infected patients with sufficient availability of peripheral blood mononuclear cells (PBMCs). We stimulated PBMCs directly *ex vivo* with pools of overlapping peptides representing ZIKV structural proteins [capsid (cap), pre-membrane (prM) and envelope (env)], as well as non-structural

proteins (NS1 to NS5). Using intracellular cytokine staining (ICS) assays, we monitored the presence of activated (CD154+CD4+ and CD69+CD8+) IFNγ-producing ZIKV-specific CD4+ and CD8+ T cells (Fig. 3a). We detected ZIKV-specific CD4+ T cells broadly targeting epitopes across the ZIKV genome, whereas CD8+ T cell responses were focused on non-structural Zika proteins (Fig. 3b). This was observed for the breadth of the response, with only 15/47 (31.9%) CD8 assays using structural antigens were positive, compared to 58/79 (73.4%) assays for NS1 to NS5 (p=0.01). In contrast CD4 responses targeted equally structural (35/47, 74.4%) and non-structural proteins (53/79, 67%) (Fig. 3c). The difference was even more pronounced for the magnitude of the response, with CD8+ T cell targeting NS1 to NS5 being almost universally one log or higher in frequency compared to those targeting structural proteins, a difference that far exceeds the difference in size of the two viral regions. (Fig. 3d). In contrast, CD4+ responses were more evenly distributed between structural and non-structural proteins. The results also indicate a differential targeting between individual ZIKV proteins, the moist obvious being the absence of CD8+ response targeting prM, but patterns were overall heterogeneous and likely confounded by different protein size. There are limited and conflicting data in the literature from ZIKV infection regards the preferred viral target regions for virus-specific CD4+ and CD8+ T cell responses, with results from human studies [24,27] as well as mice [45,46] not being consistent. Most notably a human study by Grifoni *et al.* found fewer ZIKV-specific CD8+ T cell responses targeting non-structural proteins in DENV seronegative patients, where CD8+ T cell responses to NS3–5 clearly dominate in DENV infection. Our results are more similar to the CD8+ T cell response pattern reported for DENV, with both breadth and magnitude of the CD8+ response strongly biased towards non-structural proteins, most notably NS5. Indeed, CD8+ T cell responses targeting non-structural ZIKV proteins made up at least 90% of the overall response in all patients and at most timepoints studied. In contrast, ZIKV-specific CD4+ T cell responses were much more broadly directed across the ZIKV polyprotein, with frequent recognition of capsid, envelope, NS1, NS3 and NS5 across all patients. This is different from the more capsid and envelope focused CD4+ response described for DENV. We also were unable to detect ZIKV-specific CD4+ T cells with a cytotoxic profile, as previously reported in DENV infection, suggesting that the CD4+ response might be of different quality in the two infections[47,48].

When we compared the patterns and kinetics of the T cell responses between patients with and without previous DENV exposure, the most notable observation was a strikingly strong and focused CD8+ T cell response in the DENV experienced patient CR8603, with almost 8% of CD8+ T cells targeting NS5 at the earliest timepoint, more than 1 log higher than the next biggest single protein CD8+ T cell response at any timepoint in all other patients (Fig. 3b). In addition, the patient also mounted most of the strongest CD4+ and CD8+ responses against other ZIKV proteins throughout the observation period. In contrast, the other patients with prior DENV exposure were not significantly different in their T cell response profile. There were also little phenotypic or functional differences between ZIKV-specific T cells from DENV naïve and experienced patients that would indicate a difference in speed or direction of T cell differentiation. In all patients, ZIKV-specific CD4+ T cell responses displayed a mix of mostly effector phenotype (EM: CCR7−CD45RA−) with some central-memory component (CM: CCR7+CD45RA−) evolving toward a dominant central-memory

T cell phenotype by the end of follow-up (Fig. 4a and Extended Data Fig. 6a). ZIKV-specific CD8+ T- cells were also mostly effector-memory during the acute phase, but with recovery shifted towards a phenotype with many cells re-expressing CD45RA as in terminally differentiated effector-memory T cells (TEMRA: CCR7−CD45RA+) (Fig. 4b and Extended Data Fig. 6b). Functionally, the majority of ZIKV-specific CD4+ T cells produced TNFα exclusively, with more polyfunctional ZIKV-specific CD4+ T cell responses emerging over time by additional production of IFNγ and IL-2 (Fig. 4c,d and Extended Data Fig. 7a). In contrast, ZIKV-specific CD8+ T cells mostly produced CD107a together with one or both of the cytokines IFNγ and TNFα, with resolution of infection being associated with an increase in TNFα producing cells (Fig. 4c,e and Extended Data Fig. 7b). In this context, it is important to differentiate between the general activation of CD8+ T cells as displayed in Fig. 1d and the much smaller populations of truly ZIKV-specific CD8+ T cells (Fig. 3 and 4). While the latter are thought to be key mediators of viral control and clearance, there is increasing evidence that activation of large non-specific T cell populations is a frequent phenomenon in acute viral infection and can mediate disease symptoms and tissue pathology [49-52]. Together, the data demonstrate different targeting of ZIKV regions by ZIKV-specific CD4+ versus CD8+ responses and suggest that prior DENV exposure can be associated with the rapid expansion of pre-existing DENV-specific T cells, though this seems not a universal feature in DENV seropositive patients, as also observed in a study by Grifoni *et al.*[24]. The exact extent of T cell crossreactivity between DENV and ZIKV will need to be established by larger cohort studies in natural infection, but also post vaccination.

It is worth noting that our T cell data need to be interpreted in the context of some limitations, most notably the sample size of our cohort. At this moment in time, larger cohorts of patients with acute ZIKV infection are impossible to establish, given the current absence of ZIKV outbreaks that would allow recruitment of new patient cohorts with large-volume PBMC collection. Nevertheless, our results for both CD4+ and CD8+ T cell responses were rather homogenous not only between the patients we analyzed, but also between responses targeting different viral proteins (Extended Data Fig. 8), increasing the likelihood that these results present general patterns. There is also a limitation in that none of our patients were male, thus making it impossible to identify sex-related differences in our study. Finally, in a human study it is not feasible to study immune responses beyond the blood compartment since there is no indication for any tissue biopsies in ZIKV infection. As it is well established that T cell responses in different infected tissues differ in phenotype and function from those in the blood, such studies are highly desirable but will have to be performed in animal models.

In conclusion, our comprehensive analysis of immune responses from acute symptomatic ZIKV virus infection in women finds a rapid evolution from broad and strong non-specific immune activation to the emergence of adaptive immunity by ZIKV antibodies and virus-specific CD4+ and CD8+ T cells, all within a few days after the onset of symptoms, as summarized schematically in Extended Data Fig. 9. These immune responses are not only associated with symptomatic disease, but also with almost complete control of ZIKV replication. For the T cell response, we find strikingly different target regions between virus-specific CD4+ and CD8+ T cells, with evident gaps in the CD8+ response to structural proteins. Finally, we find previous DENV infection to broadly affect the humoral response,

with effects on the T cell side limited to increased ZIKV-specific CD8+ T cell frequencies in few select patients. More detailed analyses of *Flavivirus* cross-reactive immune responses in different infection scenarios will be required in order to judge their impact on disease pathogenesis of ZIKV infection and vaccination.

Methods

Human subjects and specimen collection

Ten female subjects with acute-ZIKV infection were recruited at the Viral Hepatitis Ambulatory Clinic, Oswaldo Cruz Foundation, Rio de Janeiro, Brazil. Acute ZIKV infection was confirmed by plasma and urine detection of ZIKV RNA as well as serological detection of anti-ZIKV IgM and/or IgG antibodies. The initiation date and duration of symptoms were reported by the patients at admission. All patients were negative for other infections such as viral hepatitis (A, B, C), HIV, chikungunya and Dengue viruses as based on the absence of detection of any other viruses as well as the lack of serological evidences for another ongoing acute infection. Previous exposure to DENV (DENV pre-exposed) was defined by the positive detection of anti-DENV IgG at admission. Plasma and PBMC samples were collected at different time points as described in Fig. 1b. Additionally, urine and vaginal fluid (VF) samples may have been collected. None of the patients were pregnant at the time of the study. Nine healthy subjects have been recruited as control. This study was approved by Partners Healthcare Human Research Committee and the IRB of the Oswaldo Cruz Institute in Rio de Janeiro, Brazil, and all patients provided written informed consent.

ZIKV RNA detection and quantification

ZIKV RNA detection was performed using the internally controlled AccuPower® ZIKV Real-Time RT-PCR Kit (Bioneer Corporation, Daejeon, Republic of Korea), and a standard curve was prepared using the 1st World Health Organization (WHO) International Standard (IS) for Zika virus RNA (11468/16)[53]. Data were expressed as in international unit per 500 microliters (IU/500 μL). The WHO IS was reconstituted in accordance with the instructions for use in sterile nuclease free water and was diluted in either plasma or urine to create a standard curve. The assay has a 95% cut-off of ~80 IU/mL for both plasma and urine. For analysis of the plasma or urine samples, RNA extraction was performed using the ExiPrep™ Dx Viral RNA Kit (Bioneer Corporation) on the ExiPrep™ 16 Dx platform and PCR set-up was performed using the ExiSpin™ device (Bioneer Corporation). Amplification/detection reactions were performed using the Exicycler™ 96 Real-Time Quantitative Thermal Block (Bioneer Corporation).

ZIKV-specific antibody detection by ELISA

Presence of human anti-ZIKV IgM, IgA and IgG in plasma was detected using the DIACHECK anti-human ZIKV antibody assay, based on a viral lysate containing structural and non-structural proteins including the NS1 protein [commercially available for research use only (RUO), Dr. Julio Moran Laboratories, Zurich, Switzerland]. EuroImmun ELISA assays (EuroImmun AG, Lübeck, Germany), based on a ZIKV-specific NS1 antigen detection, were also used for the detection of anti-ZIKV IgM and IgG in plasma samples. Assays were performed in accordance with the manufacturer's instructions.

ZIKV neutralization: Endpoint method

Neutralization reactions were setup by mixing 50-μL virus (1×10^5 TCID50/mL of ZIKV Polynesian strain PF13/251013–1)[54] with 400 μL from 1:2 dilution series of heat-treated (56°C, 30min) plasma. After 2 h at 37°C, the mixtures were inoculated on 96-well plates with Vero-E6 cells (8 aliquots with 50 μL from each neutralization reaction per well). After incubation for 1 h at 37°C, 150μl D-MEM was added per well. The infection status of individual cell cultures was determined by light microscopy after 7 days. The endpoint plasma titer resulting in neutralization (i.e., no infection) of 50% of cell cultures (NT50) was calculated by maximum likelihood algorithm.

Immunophenotyping by flow cytometry

For the profiling of the different immune subsets presented in Fig. 1d, surface staining of PBMCs was performed as follows: In brief, cells were thawed and washed in R10 medium [RPMI 1640 (Sigma-Aldrich), 2% FCS, 1.5% 1M HEPES buffer (Fisher Scientific), L-glutamine 1X (Fisher Scientific) and Streptomycin/penicillin 1X (Fisher Scientific)]. Cells were then stained with LIVE/DEAD Cell Viability dye (Thermo Fisher Scientific) according to the manufacturer's protocol. Cells were washed in FACS buffer and stained for surface antibodies: [CD16-BUV395 (clone 3G8, BD Biosciences); CD14-AF700 or CD14-APC-Cy7 (clone UCD14, Biolegend); HLA-DR-BV605 (clone L243, Biolegend); CD123-APC (clone 6H6, Biolegend); CD11c-PerCP-Cy5.5 (clone 3.9, Biolegend); CD33-PE (clone P67.6, Biolegend); CD11b-PE/Dazzle 594 (clone ICRF44, Biolegend); CD27-PE-Texas Red (clone O323, Biolegend); CD38-PE-Cy7 (clone HB7, eBioscience); CD3-BUV496 (clone UCHT1, BD Biosciences); CD3-AF700 (clone UCHT1, Biolegend); CD19-BUV496 (clone SJ25C1, BD Biosciences); CD4-APC (clone RPA-T4, Biolegend); CD8-PE (clone RPA-T8, Biolegend); and CD56-APC-Cy7 (clone HCD56, Biolegend)]. Following surface antigen staining, cells were washed twice in FACS buffer and fixed in 4% Paraformaldehyde solution (Affymetrix). All steps were performed at 4°C, unless specified otherwise by the manufacturer. Acquisition was performed on an LSR-II flow cytometer (Becton Dickinson) and data were analyzed using FlowJo software.

Intracellular cytokine staining assays

Frozen PBMC samples were rested overnight at 37°C in R10 medium [RPMI 1640 (Sigma-Aldrich), 2% FCS, 1.5% 1M HEPES buffer (Fisher Scientific), L-glutamine 100X (Fisher Scientific) and Streptomycin/penicillin 50X (Fisher Scientific)]. Cells were counted and distributed at 3 million cells per condition. For each PBMC samples, 9 different conditions were tested: one unstimulated condition and eight stimulated conditions with eight 15-mer overlapping-peptide pools covering ZIKV capsid (cap), pre-membrane (prM), envelope (env), non-structural protein 1 (NS1), NS2A + NS2B, NS3, NS4A+2k+NS4B and NS5 (JPT Peptide Technologies, Berlin, Germany or A&A, San Diego, CA). Stimulation was performed in the presence of 10 μL/mL anti-CD28/49d (BD Biosciences), 5μl of CD107a-BV421antibody (clone H4A3, Biolegend) and 5 μg/mL of peptides (except for the unstimulated condition), in R10 medium to a final volume of 500 μL. Additionally, 1X Cell Stimulation Cocktail of PMA and Ionomycine has been used as a positive control (eBioscience™). Cells were incubated for 6 hours at 37°C and 1X Protein Transport

Inhibitor (eBioscience™) was added after the 2 first hours of incubation. At the end of the incubation time, cells were washed and stained with a viability dye (LIVE/DEAD Fixable Blue; Thermo Fisher Scientific) according to the manufacturer's protocol, then with the following surface antibodies and as described above: CD3-AF700 (clone UCHT1, Biolegend); CD4-PE-Cy7 (clone RPA-T4, Biolegend); CD8-BUV395 (clone RPA-T8, Biolegend); CD45RA-AF700 (clone HI100, Biolegend); CCR7−PE (clone G043H7, Biolegend); CD19-BUV496 (clone SJ25C1, BD Biosciences). After surface antigen staining, cells were washed twice in FACS buffer and fixation/permeabilization step was performed using the FOXP3 Transcription Factor Staining buffer set, according to manufacturer's protocol. The following antibodies were used for intracellular staining: CD69-BV510 (clone FN50, Biolegend); CD154-AF488 (clone 24–31, Biolegend); IFNγ-APC-Cy7 (clone 4S.B3, Biolegend); TNFα-BV605 (clone MAb11, Biolegend); IL-2-APC (clone MQ1–17H12, BD Biosciences). All steps were performed at 4°C, unless specified otherwise by the manufacturer. Acquisition was performed on an LSR-II flow cytometer (Becton Dickinson) and data were analyzed using FlowJo (FlowJo LLC) and Spice (NIAID) software. The unstimulated condition was used to subtract any background staining in the analysis and positive ICS were determined by the detection of at least 10 ZIKV-specific T cells and a frequency of ZIKV-specific T cells of at least twice the corresponding unstimulated signal.

Extended Data

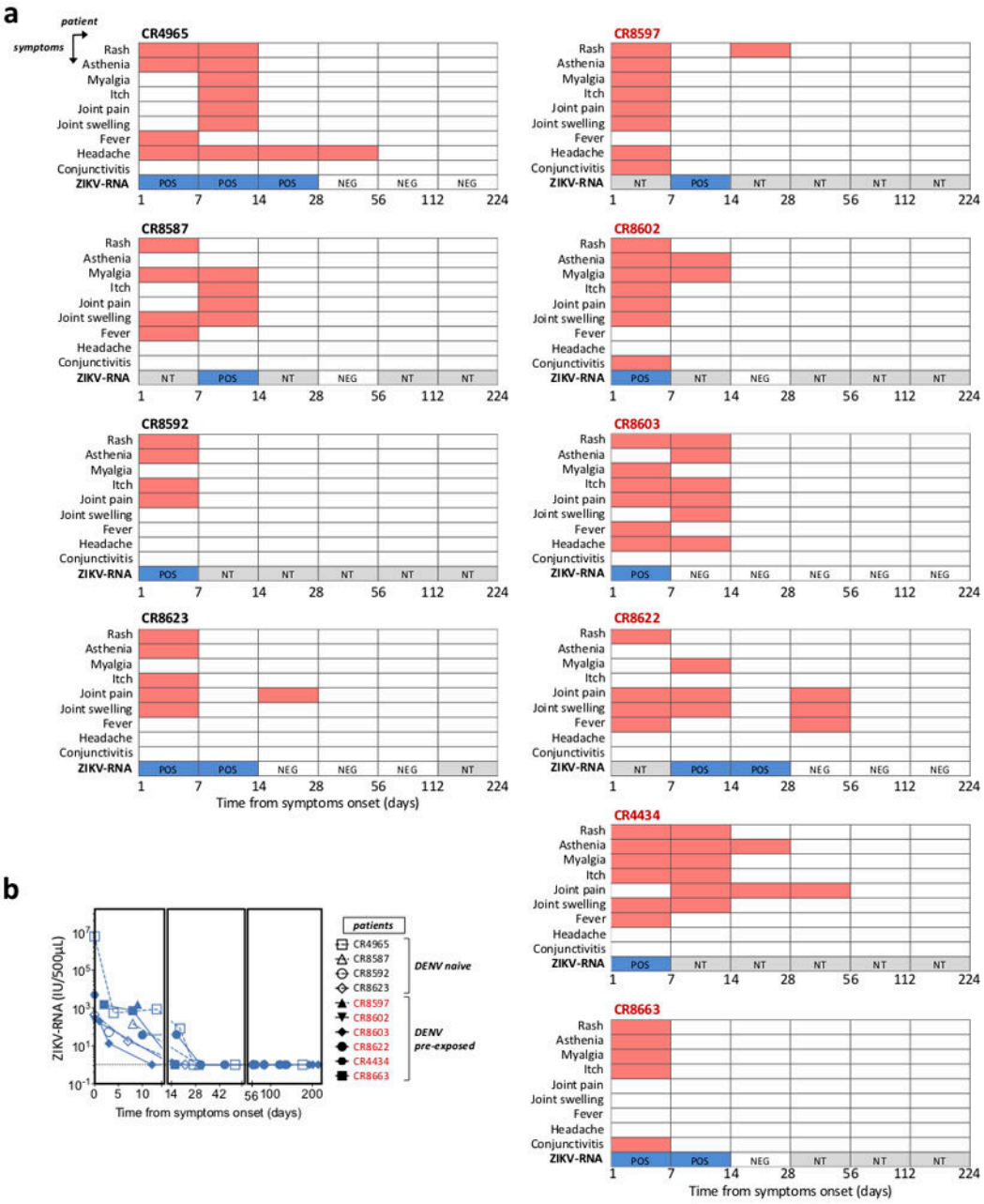

Extended Data Fig. 1. Patient's symptoms and ZIKV-RNA detection data

(a) Patient's symptoms information and associated plasma ZIKV-RNA detection, over time. (**b**) Quantification of ZIKV RNA in the plasma. Each patient and previous exposure to DENV status, as defined by the positive detection of anti-DENV IgG at symptom onset, is displayed through unique symbols and connecting lines. X-axis, Time (days) represents the time from onset of symptoms. Gray dashed line notes the assay's detection limit. Data are representative of n=2 independent experiments.

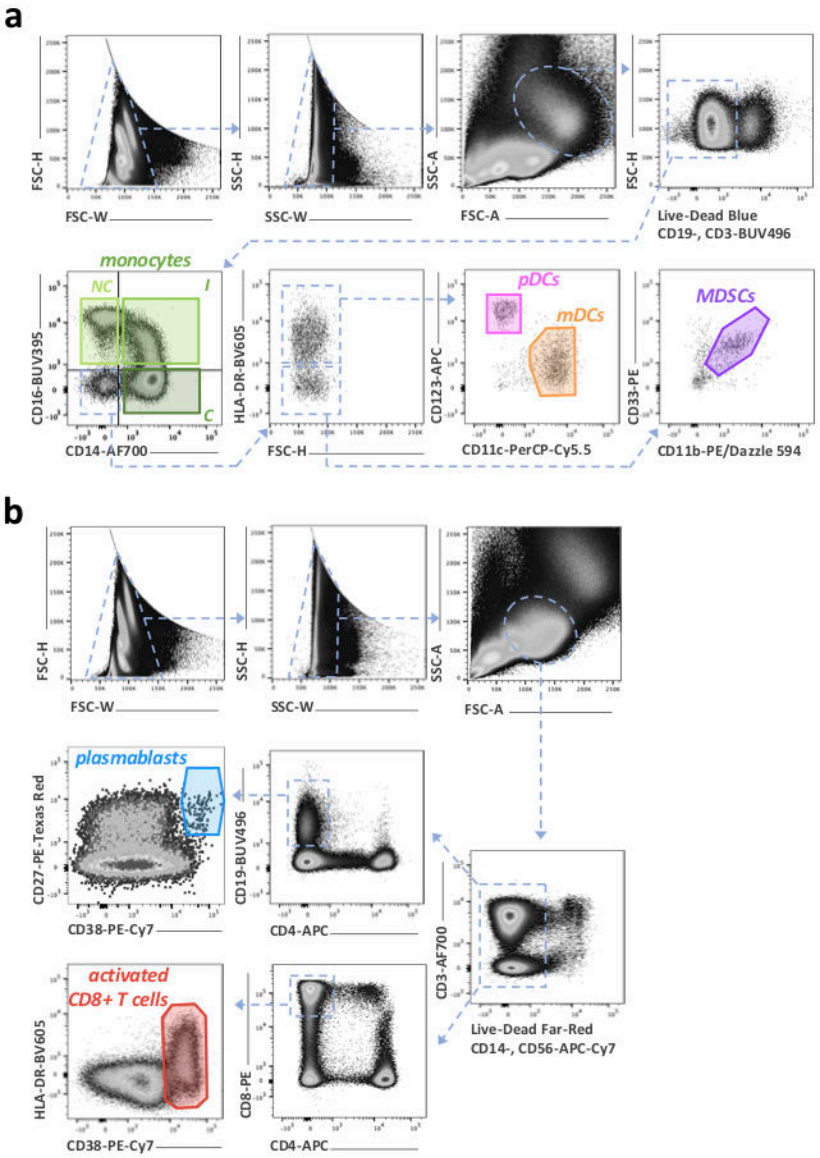

Extended Data Fig. 2. Gating strategies for blood immunophenotyping

Flow cytometry gating strategies for the identification of the different cell subsets of monocytes (NC= non-classical; I= intermediate; C= classical), dendritic cells (pDCs= plasmacytoid dendritic cells; mDCs= myeloid dendritic cells) and MDSCs (myeloid-derived suppressor cells) (**a**), as well as plasmablasts and activated CD8+ T cells (**b**).

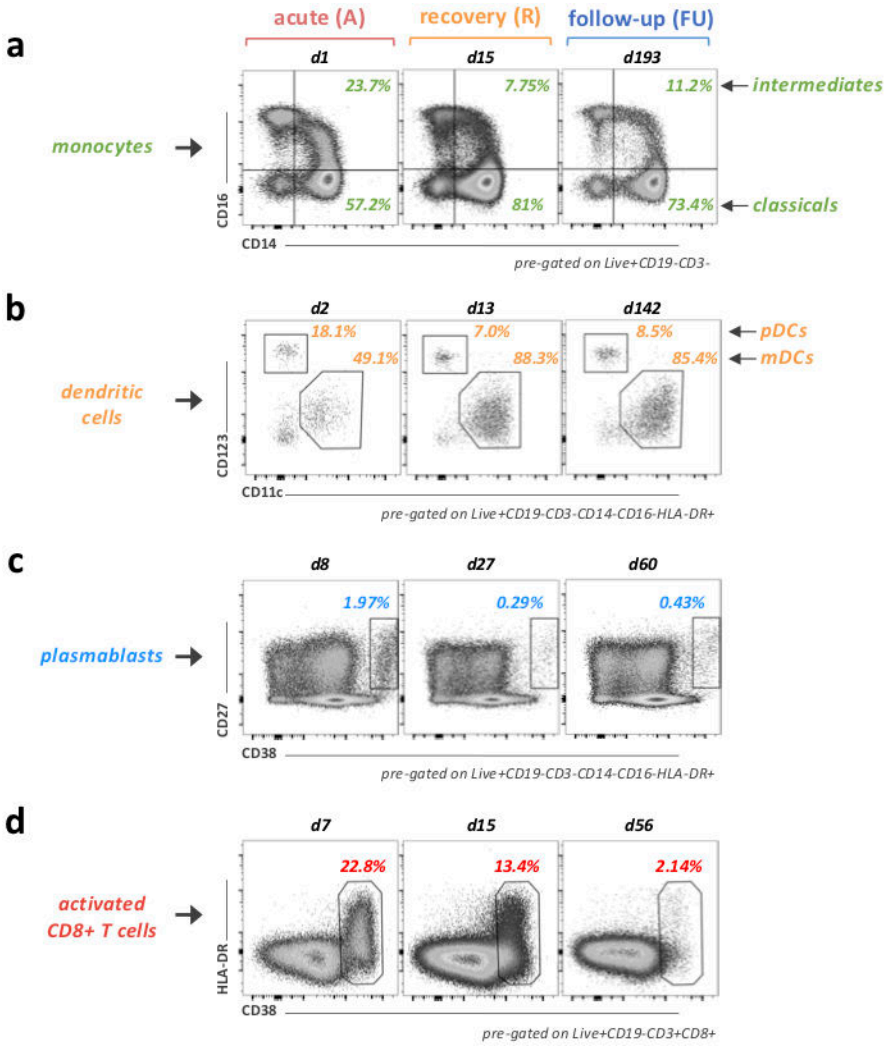

Extended Data Fig. 3. Changes in immune cell frequencies following acute ZIKV infection

Representative flow-cytometry plots showing changes in the frequency of monocytes (**a**), dendritic cells (**b**), plasmablasts (**c**) and activated CD8+ T cells (**d**), at different time points following ZIKV infection. Numerical values of the measured frequencies in a total n=10 patients, at different time points (acute n=10; recovery n=5; follow-up n=4) are displayed in Fig. 1d. Times (in days) from onset of symptoms are indicated.

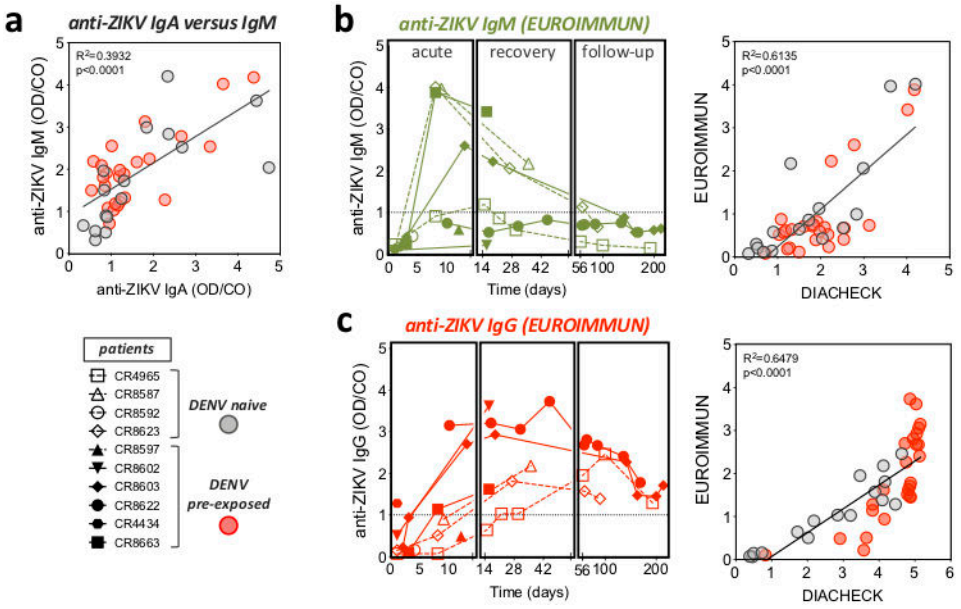

Extended Data Fig. 4. Humoral immune response to acute ZIKV infection

Linear regression analysis to model the relationship between plasma anti-ZIKV IgM and IgA detection signals (n=41) using DIACHECK ELISA assays. (**b**) Plasma detection of anti-ZIKV IgM antibodies using EUROIMMUNE ELISA assay (left chart) and linear regression analysis to model the relationship between plasma anti-ZIKV IgM detection signals obtained with EUROIMMUNE and DIACHECK ELISA assays (n=41) (right chart). (**c**) Plasma detection of anti-ZIKV IgG antibodies using EUROIMMUNE ELISA assay (left chart) and linear regression analysis to model the relationship between plasma anti-ZIKV IgG detection signals obtained with EUROIMMUNE and DIACHECK ELISA assays (n=41) (right chart). (**a-c**) Each patient and previous exposure to DENV status, as defined by the positive detection of anti-DENV IgG at symptom onset, is displayed through unique symbols and connecting lines. Gray dashed lines note assay's detection limits. X-axis, (Time (days)) represents the time from onset of symptoms. Data are expressed as mean values of OD/CO ratios from two independent experiments. Pearson correlation coefficient *R* and significance *p* (two-sided) values are reported from the linear regression analysis performed with GraphPad Prism software.

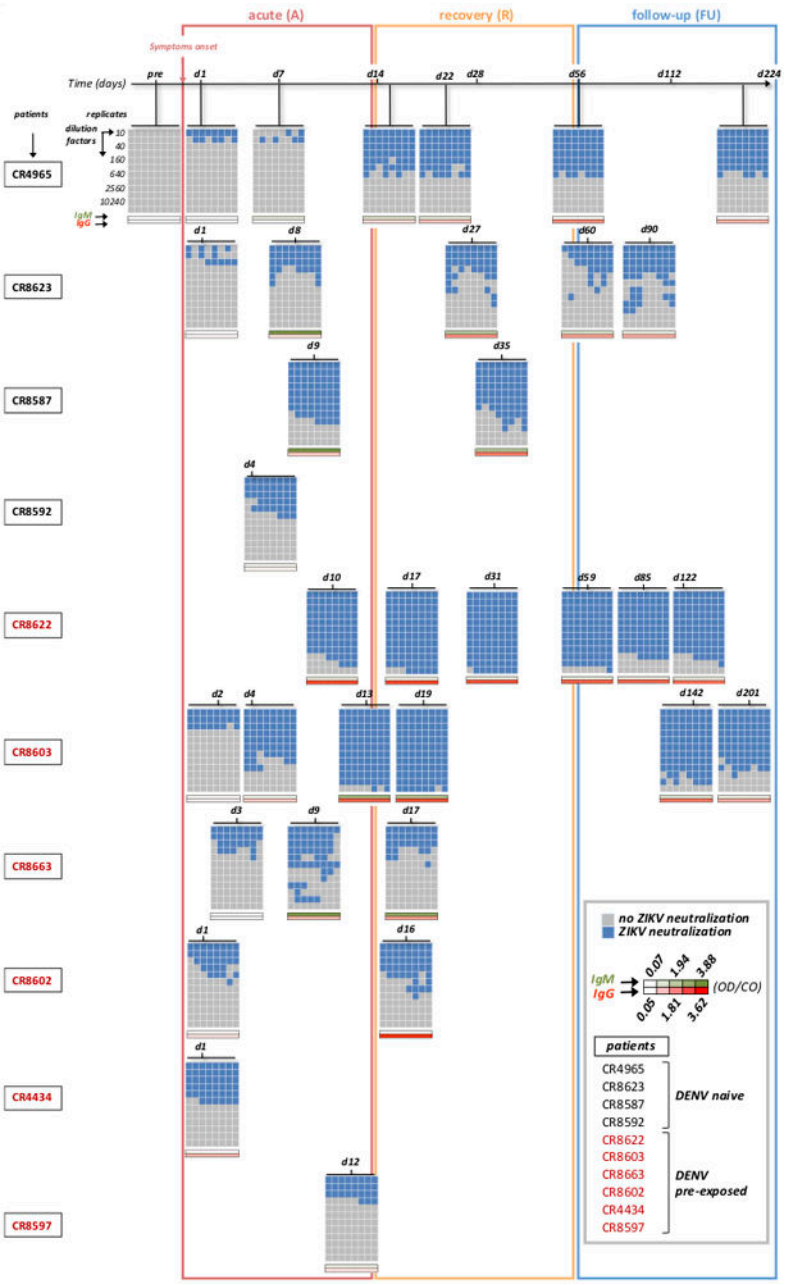

Extended Data Fig. 5. Titration of anti-ZIKV neutralizing antibodies

Representative titration assays for the detection of anti-ZIKV neutralizing antibodies, overtime. Titers were measured by endpoint titration. A color mapping of the OD/CO ratio values for the detection anti-ZIKV IgM and IgG using EUROIMUNE ELISA assays are indicated. The data are representative of n=2 (patients CR8587, CR8602, CR8663, CR4434, CR8597 and CR8622), n=3 (patients CR4565 and 8603) or n=4 (CR8623) independent experiments.

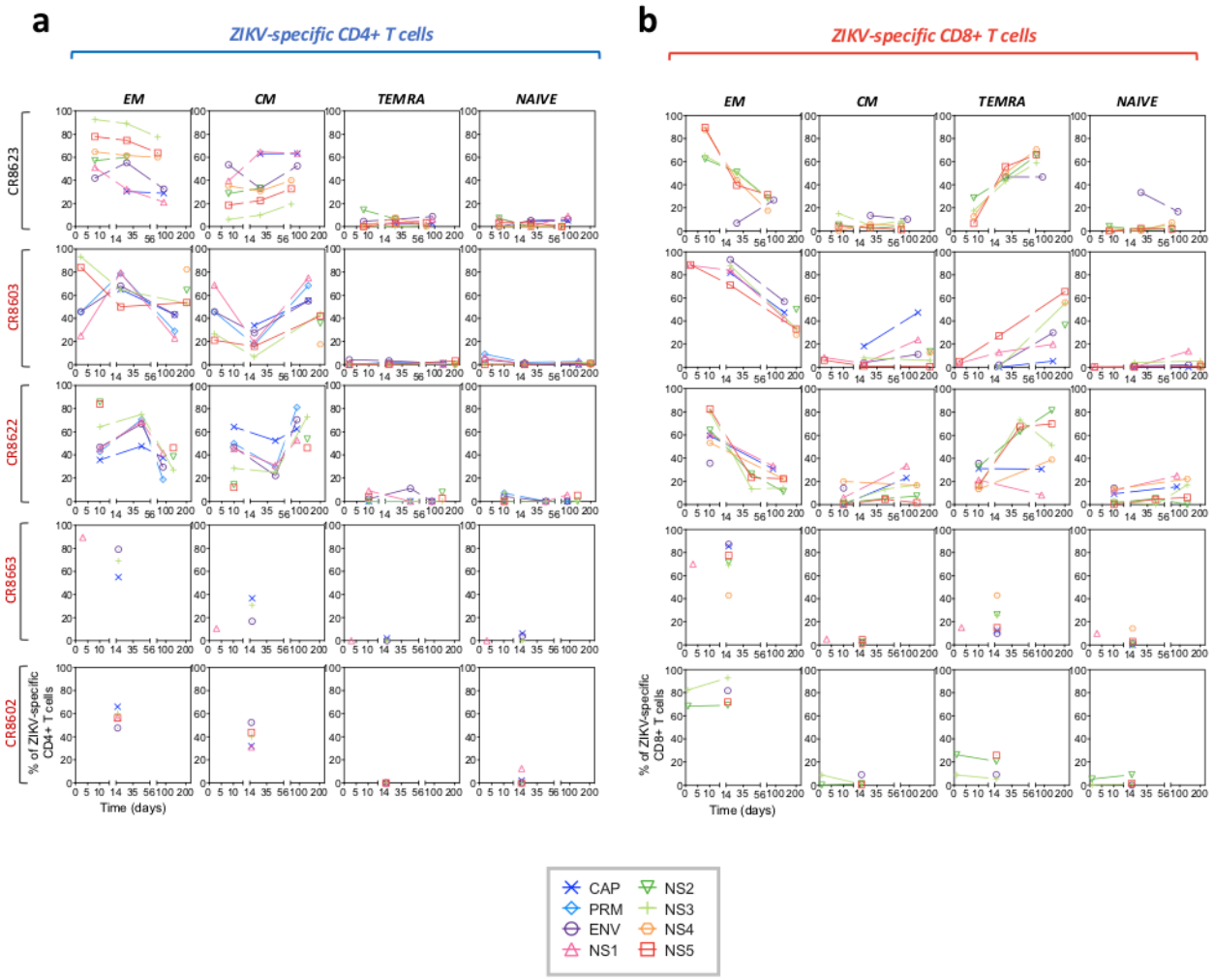

Extended Data Fig. 6. ZIKV-specific T cell memory differentiation following acute ZIKV infection

T cell memory differentiation based on CCR7 and CD45RA co-expression (naïve: CCR7+CD45RA+; CM: CCR7+CD45RA-; EM: CCR7−CD45RA−; TEMRA: CCR7−CD45RA+). Frequencies of ZIKV-specific CD4+ (**a**) and CD8+ (**b**) T cells across the different memory subsets over time, from 5 different patients, are indicated. The analysis was performed on a total of n=6 patients, at different time points (Data from patient CR4965 are available in Fig. 4a,b).

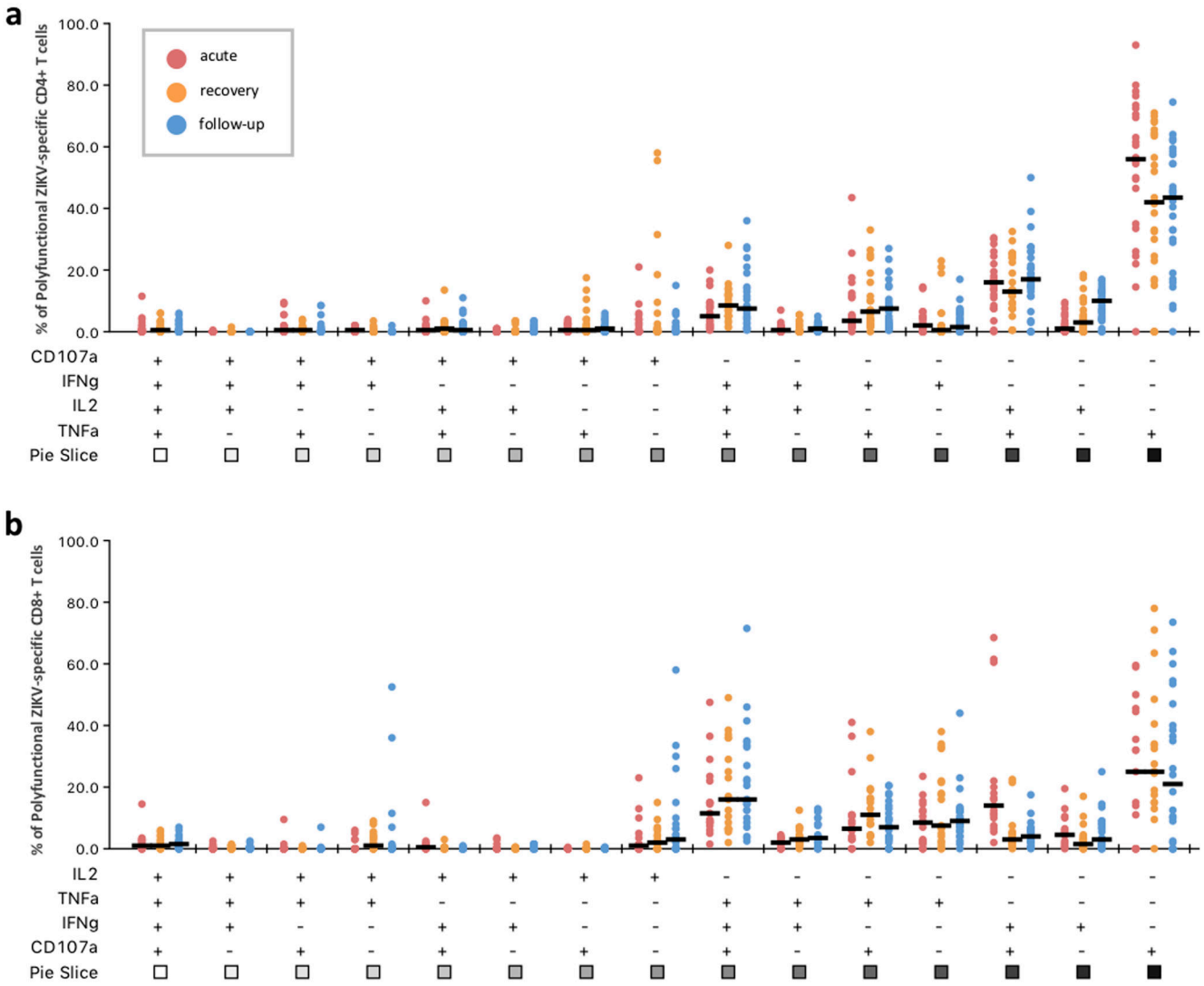

Extended Data Fig. 7. ZIKV-specific T cell functional profiles overtime

Detailed representation of the overlapping pie charts presented in Fig. 4d,e. The data represent the different sub-groups of cytokine secreting and cytotoxic CD154+CD4+ (**a**) and CD69+CD8+ (**b**) T cells after stimulation with 15-mer overlapping peptide pools covering all ZIKV-proteins, by *ex vivo* intracellular cytokine stainings (ICSs). Frequencies of IL-2, TNFa, IFNγ and CD107a co-expressing cells are indicated. Baseline signals of IL-2, TNFα, IFNγ and CD107a-expressing cells from unstimulated controls have been subtracted to the stimulated conditions to allow the visualization of ZIKV-specific CD4+ and CD8+ T cell signals. Only time points with detectable CD154+IFNγ+CD4+ (acute n=24, recovery n=26, follow-up n=29) and CD69+IFNγ+CD8+ T cells (acute n=17, recovery n=19, follow-up n=24) from patients CR4965, CR8623, CR8603 and CR8622, as depicted in Fig. 3a,b, have been used for this analysis. Black bars correspond to the median of expression in each condition.

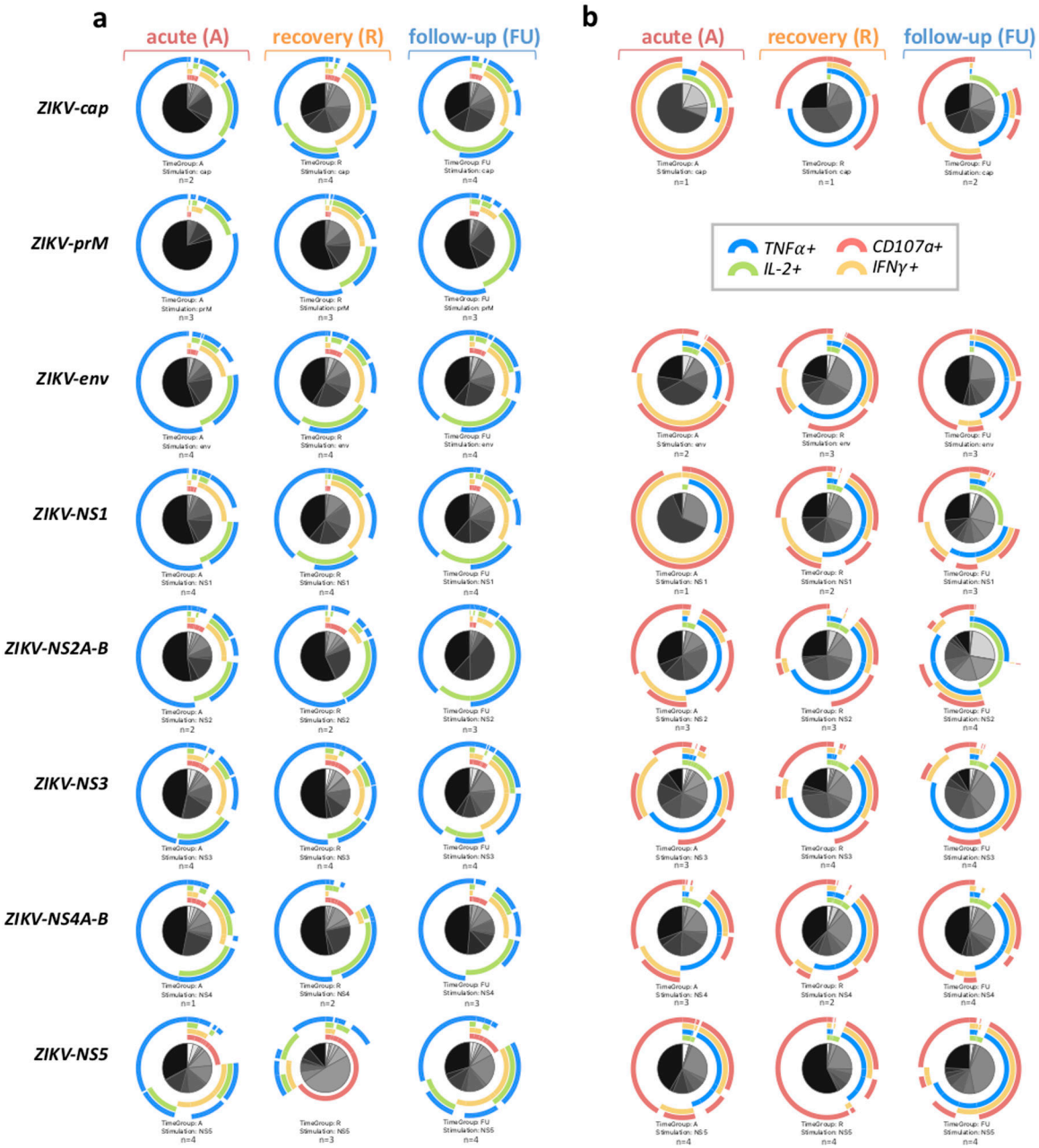

Extended Data Fig. 8. ZIKV-specific T cell functional profiles across the different viral proteins targeted

Overlapping pie charts describing the polyfunctionality of ZIKV-specific CD4+ (**a**) and CD8+ (**b**) T cells according to the ZIKV-overlapping peptide pools used for T cell stimulation and determined by *ex vivo* intracellular cytokine staining (ICS) as defined in Fig. 3. Baseline signals of TNFα, IL-2, CD107a and IFNγ-producing cells in unstimulated controls have been subtracted from ZIKV-stimulated assays to allow the visualization of ZIKV-specific CD4+ and CD8+ T cell signals. Only time points with detectable CD154+IFNγ+CD4+ (acute n=24, recovery n=26, follow-up n=29) and CD69+IFNγ +CD8+ T cells (acute n=17, recovery n=19, follow-up n=24) from patients CR4965,

CR8623, CR8603 and CR8622, as depicted in Fig. 3a,b, were used for this analysis. Distribution of the numbers (n) of T cell responses across the different ZIKV-peptide pools are reported.

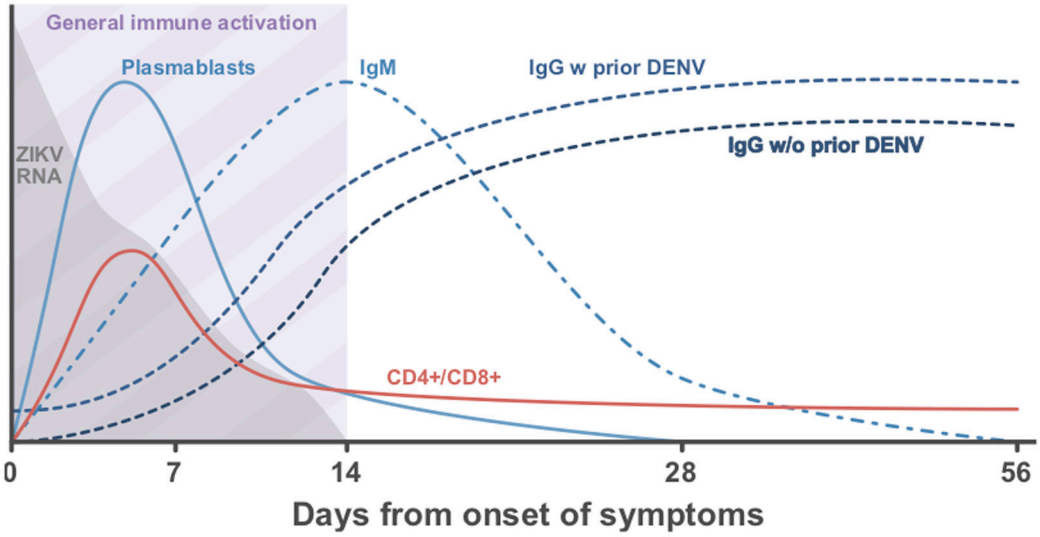

Extended Data Fig. 9.

General overview of the dynamics of immune responses following acute ZIKV infection in human.

Extended Data Table 1.

Patient's demographics and HLA-types

patient ID	Sex	Age	HLA-A I	HLA-A II	HLA-B I	HLA-B II	HLA-DRB1 I	HLA-DRB1 II
CR4965	F	31	A*24:02	A*68:02	B*52:01	B*53:01	DRB1*01:02	DRB1*08:07
CR8587	F	31	A*29:02	A*68:02	B*13:02	B*44:03	DRB1*07:01	DRB1*07:01
CR8592	F	27	A*02:05	A*33:01	B*44:03	8*49:01	DRB1*07:01	DRB1*11:02
CR8623	F	33	A*02:01	A*68:02	B*27:05	B*35:02	DRB1*07:01	DRB1*11:04
CR8597	F	44	A*02:01	A*36:01	8*51:01	B*53:01	DRB1*11:01	DRB1*15:03
CR8602	F	49	A*02:01	A*02:11	B*48:02	B*50:01	DRB1*07:01	DRB1*08:04
CR8603	F	50	A*02:01	A*02:01	B*18:01	B*35:01	DRB1*01:03	DRB1*03:01
CR8622	F	28	A*03:01	A*68:01	B*14:XX	B*18:XX	DRB1*12:01	DRB1*13:01
CR4434	F	42	A*02:01	A*03:01	B*07:02	B*07:02	DRB1*08:04	DRB1*15:01
CR8663	F	56	A*02:01	A*30:02	B*07:02	B*14:02	DRB1*14:01/54	DRB1*15:03

Supplementary Material

Refer to Web version on PubMed Central for supplementary material.

Acknowledgements:

We would like to acknowledge the patients as well as the physicians and medical staff of the Viral Hepatitis Clinic in Brazil who provided care to the patients. We also would like to acknowledge the Flavivirus Laboratory staff at FIOCRUZ as well as Dr. Joshua Quick and Pr. Nicholas Loman from the university of Birmingham for their assistance in analyzing patient's samples for ZIKV detection. We thank Bruna da Silva Baptista as well as the Massachusetts General Hospital HSCI CRM flow cytometry core facility members for their technical assistance. This work was supported in parts by National institutes of health grants U01 AI131314 (to GML and LLLX), U19 AI082630 (to GML and LLLX), HHSN27220140045C (to AS), 1PO1AI106695–01A1 (to AS), U19AI118626–01 (to AS), 75N9301900065 (to AS), the EU-grant 734584 (to AS), Conselho Nacional de Desenvolvimento

Tecnológico (CNPq # 470092/2014–9; #200099/2016–7), Fundação de Amparo à Pesquisa do Estado do Rio de Janeiro (Faperj E-26/202.930/2016) and “Sicherheit von Blut(produkten) und Geweben hinsichtlich der Abwesenheit von Zikaviren” from the German Ministry of Health.

References

1. Ye Q et al. Genomic characterization and phylogenetic analysis of Zika virus circulating in the Americas. Infect. Genet. Evol 43, 43–49 (2016). [PubMed: 27156653]
2. Kraemer MUG et al. The global distribution of the arbovirus vectors Aedes aegypti and Ae. albopictus. Elife 4, e08347 (2015). [PubMed: 26126267]
3. Simeone RM et al. Possible Zika Virus Infection Among Pregnant Women - United States and Territories, May 2016. MMWR Morb. Mortal. Wkly. Rep 65, 514–519 (2016). [PubMed: 27248295]
4. Meaney-Delman D et al. Zika Virus Infection Among U.S. Pregnant Travelers - August 2015-February 2016. MMWR Morb. Mortal. Wkly. Rep 65, 211–214 (2016). [PubMed: 26938703]
5. Foy BD et al. Probable non-vector-borne transmission of Zika virus, Colorado, USA. Emerging Infect. Dis 17, 880–882 (2011). [PubMed: 21529401]
6. Musso D et al. Potential sexual transmission of Zika virus. Emerging Infect. Dis 21, 359–361 (2015). [PubMed: 25625872]
7. Motta IJF et al. Evidence for Transmission of Zika Virus by Platelet Transfusion. N. Engl. J. Med 375, 1101–1103 (2016). [PubMed: 27532622]
8. Petersen LR, Jamieson DJ, Powers AM & Honein MA Zika Virus. N. Engl. J. Med 374, 1552–1563 (2016). [PubMed: 27028561]
9. Osuna CE et al. Zika viral dynamics and shedding in rhesus and cynomolgus macaques. Nat. Med 22, 1448–1455 (2016). [PubMed: 27694931]
10. Bonaldo MC et al. Isolation of Infective Zika Virus from Urine and Saliva of Patients in Brazil. PLoS Negl Trop Dis 10, e0004816 (2016). [PubMed: 27341420]
11. Sotelo JR et al. Persistence of Zika Virus in Breast Milk after Infection in Late Stage of Pregnancy. Emerging Infect. Dis 23, 856–857 (2017).
12. Aid M et al. Zika Virus Persistence in the Central Nervous System and Lymph Nodes of Rhesus Monkeys. Cell 169, 610–620.e14 (2017). [PubMed: 28457610]
13. Brasil P et al. Guillain-Barré syndrome associated with Zika virus infection. Lancet 387, 1482 (2016). [PubMed: 27115821]
14. Lannuzel A et al. Long-term outcome in neuroZika: When biological diagnosis matters. Neurology 92, e2406–e2420 (2019). [PubMed: 31028126]
15. Brasil P et al. Zika Virus Infection in Pregnant Women in Rio de Janeiro. N. Engl. J. Med 375, 2321–2334 (2016). [PubMed: 26943629]
16. Rasmussen SA, Jamieson DJ, Honein MA & Petersen LR Zika Virus and Birth Defects--Reviewing the Evidence for Causality. N. Engl. J. Med 374, 1981–1987 (2016). [PubMed: 27074377]
17. Costa F et al. Emergence of Congenital Zika Syndrome: Viewpoint From the Front Lines. Ann. Intern. Med 164, 689–691 (2016). [PubMed: 26914810]
18. França GVA et al. Congenital Zika virus syndrome in Brazil: a case series of the first 1501 livebirths with complete investigation. Lancet 388, 891–897 (2016). [PubMed: 27372398]
19. Hazin AN et al. Computed Tomographic Findings in Microcephaly Associated with Zika Virus. N. Engl. J. Med 374, 2193–2195 (2016).
20. Honein MA et al. Birth Defects Among Fetuses and Infants of US Women With Evidence of Possible Zika Virus Infection During Pregnancy. JAMA 317, 59–68 (2017). [PubMed: 27960197]
21. Stettler K et al. Specificity, cross-reactivity, and function of antibodies elicited by Zika virus infection. Science 353, 823–826 (2016). [PubMed: 27417494]
22. Wang Q et al. Molecular determinants of human neutralizing antibodies isolated from a patient infected with Zika virus. Sci Transl Med 8, 369ra179 (2016).

23. Robbiani DF et al. Recurrent Potent Human Neutralizing Antibodies to Zika Virus in Brazil and Mexico. Cell 169, 597–609.e11 (2017). [PubMed: 28475892]
24. Grifoni A et al. Prior Dengue virus exposure shapes T cell immunity to Zika virus in humans. J. Virol (2017). doi:10.1128/JVI.01469-17
25. Ricciardi MJ et al. Ontogeny of the B- and T-cell response in a primary Zika virus infection of a dengue-naïve individual during the 2016 outbreak in Miami, FL. PLoS Negl Trop Dis 11, e0006000 (2017). [PubMed: 29267278]
26. Lai L et al. Innate, T-, and B-Cell Responses in Acute Human Zika Patients. Clin. Infect. Dis 66, 1–10 (2018). [PubMed: 29020226]
27. Delgado FG et al. Improved Immune Responses Against Zika Virus After Sequential Dengue and Zika Virus Infection in Humans. Viruses 10, (2018).
28. Carlin AF et al. A longitudinal systems immunologic investigation of acute Zika virus infection in an individual infected while traveling to Caracas, Venezuela. PLoS Negl Trop Dis 12, (2018).
29. Michlmayr D, Andrade P, Gonzalez K, Balmaseda A & Harris E CD14+CD16+ monocytes are the main target of Zika virus infection in peripheral blood mononuclear cells in a paediatric study in Nicaragua. Nat Microbiol 2, 1462–1470 (2017). [PubMed: 28970482]
30. Foo S-S et al. Asian Zika virus strains target CD14+ blood monocytes and induce M2-skewed immunosuppression during pregnancy. Nat Microbiol 2, 1558–1570 (2017). [PubMed: 28827581]
31. Sun X et al. Transcriptional Changes during Naturally Acquired Zika Virus Infection Render Dendritic Cells Highly Conducive to Viral Replication. Cell Rep 21, 3471–3482 (2017). [PubMed: 29262327]
32. Wang C et al. Myeloid-Derived Suppressor Cells Inhibit T Follicular Helper Cell Immune Response in Japanese Encephalitis Virus Infection. J. Immunol. 199, 3094–3105 (2017). [PubMed: 28978693]
33. Everett H & McFadden G Apoptosis: an innate immune response to virus infection. Trends Microbiol. 7, 160–165 (1999). [PubMed: 10217831]
34. Shi C & Pamer EG Monocyte recruitment during infection and inflammation. Nat. Rev. Immunol 11, 762–774 (2011). [PubMed: 21984070]
35. Ishikawa T, Yamanaka A & Konishi E A review of successful flavivirus vaccines and the problems with those flaviviruses for which vaccines are not yet available. Vaccine 32, 1326–1337 (2014). [PubMed: 24486372]
36. Barouch DH, Thomas SJ & Michael NL Prospects for a Zika Virus Vaccine. Immunity 46, 176–182 (2017). [PubMed: 28228277]
37. Abbink P et al. Protective efficacy of multiple vaccine platforms against Zika virus challenge in rhesus monkeys. Science 353, 1129–1132 (2016). [PubMed: 27492477]
38. Larocca RA et al. Vaccine protection against Zika virus from Brazil. Nature 536, 474–478 (2016). [PubMed: 27355570]
39. Rogers TF et al. Zika virus activates de novo and cross-reactive memory B cell responses in dengue-experienced donors. Sci Immunol 2, (2017).
40. Dejnirattisai W et al. Dengue virus sero-cross-reactivity drives antibody-dependent enhancement of infection with zika virus. Nat. Immunol 17, 1102–1108 (2016). [PubMed: 27339099]
41. Bardina SV et al. Enhancement of Zika virus pathogenesis by preexisting antiflavivirus immunity. Science 356, 175–180 (2017). [PubMed: 28360135]
42. Pantoja P et al. Zika virus pathogenesis in rhesus macaques is unaffected by pre-existing immunity to dengue virus. Nat Commun 8, 15674 (2017). [PubMed: 28643775]
43. Terzian ACB et al. Viral Load and Cytokine Response Profile Does Not Support Antibody-Dependent Enhancement in Dengue-Primed Zika Virus-Infected Patients. Clin. Infect. Dis 65, 1260–1265 (2017). [PubMed: 29017246]
44. George J et al. Prior Exposure to Zika Virus Significantly Enhances Peak Dengue-2 Viremia in Rhesus Macaques. Sci Rep 7, 10498 (2017). [PubMed: 28874759]
45. Wen J et al. Identification of Zika virus epitopes reveals immunodominant and protective roles for dengue virus cross-reactive CD8+ T cells. Nat Microbiol 2, 17036 (2017). [PubMed: 28288094]

46. Elong Ngono A et al. Mapping and Role of the CD8+ T Cell Response During Primary Zika Virus Infection in Mice. Cell Host Microbe 21, 35–46 (2017). [PubMed: 28081442]

47. Duangchinda T et al. Immunodominant T-cell responses to dengue virus NS3 are associated with DHF. Proc. Natl. Acad. Sci. U.S.A 107, 16922–16927 (2010). [PubMed: 20837518]

48. Tian Y, Sette A & Weiskopf D Cytotoxic CD4 T Cells: Differentiation, Function, and Application to Dengue Virus Infection. Front Immunol 7, 531 (2016). [PubMed: 28003809]

49. Dung NTP et al. Timing of CD8+ T cell responses in relation to commencement of capillary leakage in children with dengue. J. Immunol 184, 7281–7287 (2010). [PubMed: 20483770]

50. Crosby EJ, Goldschmidt MH, Wherry EJ & Scott P Engagement of NKG2D on bystander memory CD8 T cells promotes increased immunopathology following Leishmania major infection. PLoS Pathog. 10, e1003970 (2014). [PubMed: 24586170]

51. Kim J et al. Innate-like Cytotoxic Function of Bystander-Activated CD8+ T Cells Is Associated with Liver Injury in Acute Hepatitis A. Immunity 48, 161–173.e5 (2018). [PubMed: 29305140]

52. Maini MK et al. The role of virus-specific CD8(+) cells in liver damage and viral control during persistent hepatitis B virus infection. J. Exp. Med 191, 1269–1280 (2000). [PubMed: 10770795]

53. Baylis SA et al. Harmonization of nucleic acid testing for Zika virus: development of the 1st World Health Organization International Standard. Transfusion 57, 748–761 (2017). [PubMed: 28229462]

54. Trösemeier J-H et al. Genome Sequence of a Candidate World Health Organization Reference Strain of Zika Virus for Nucleic Acid Testing. Genome Announc 4, (2016).

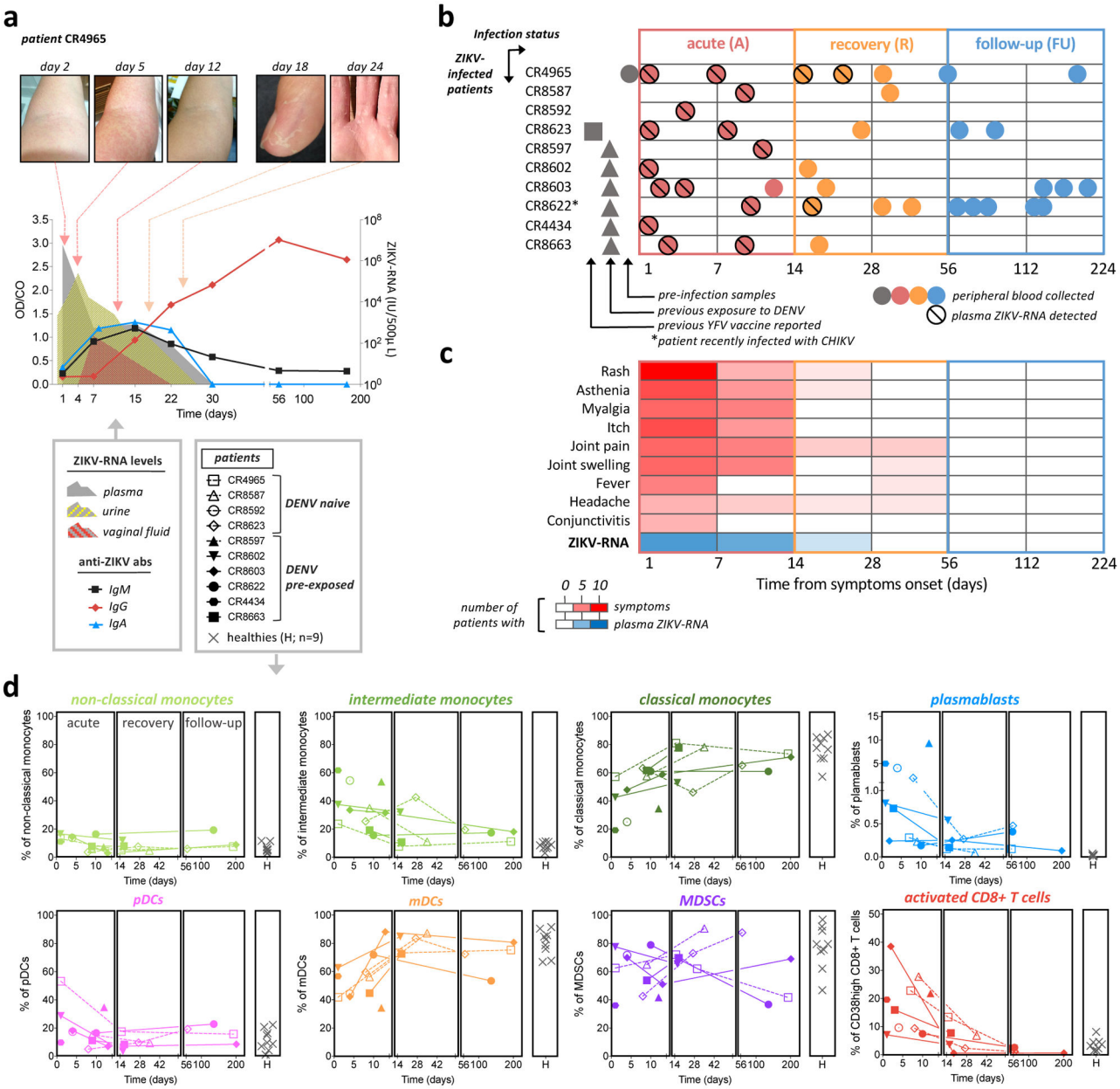

Fig. 1: Clinical and immunological features of ten ZIKV acutely-infected women.

(**a**) Complete clinical follow-up of a 31-year-old woman assessed at the Viral Hepatitis Ambulatory Clinic, Oswaldo Cruz Foundation, Rio de Janeiro, Brazil. Representative pictures of maculopapular cutaneous rash on arms and dry peeling skin on hands are depicted, as well as plasma, urine and vaginal fluid detection of ZIKV RNA, and plasma detection of anti-ZIKV IgM, IgA and IgG. (**b**) ZIKV-infected subjects and peripheral-blood specimen collection over time since symptom onset. Patients with previously documented Dengue (DENV) or Chikungunya (CHIKV) viruses or Yellow-fever (YFV) vaccine exposures are annotated. (**c**) Color mapping of the number of patients with designated symptoms or clinical signs, and who are positive for ZIKV-RNA detection in the plasma. *patient CR8622 had recent documented CHIKV infection and ZIKV-associated symptoms

onset correspond to a rebound in symptoms previously experienced following CHIKV infection, as both infections have similar symptom patterns. (**d**) Flow cytometry analysis of the frequency of the different monocyte and dendritic cell subsets, as well as of myeloid-derived suppressor cells (MDSCs), plasmablasts and activated (CD38high) CD8+ T cells, in the peripheral blood of ZIKV-infected patients at different time points starting from symptom onset (acute n=10; recovery n=5; follow-up n=4). Flow cytometry gating strategies are depicted in Extended Data Fig. 2. Data are expressed as percentages of the indicated populations. Each patient and previous exposure to DENV status, as defined by the positive detection of anti-DENV IgG at symptom onset, are displayed through unique symbols and connecting lines. Cross symbols represent data from 9 healthy adults, as a control. X-axis, Time (days) represents the time from symptom onset. Abbreviations: pDCs= plasmacytoid dendritic cells; mDCs= myeloid dendritic cells.

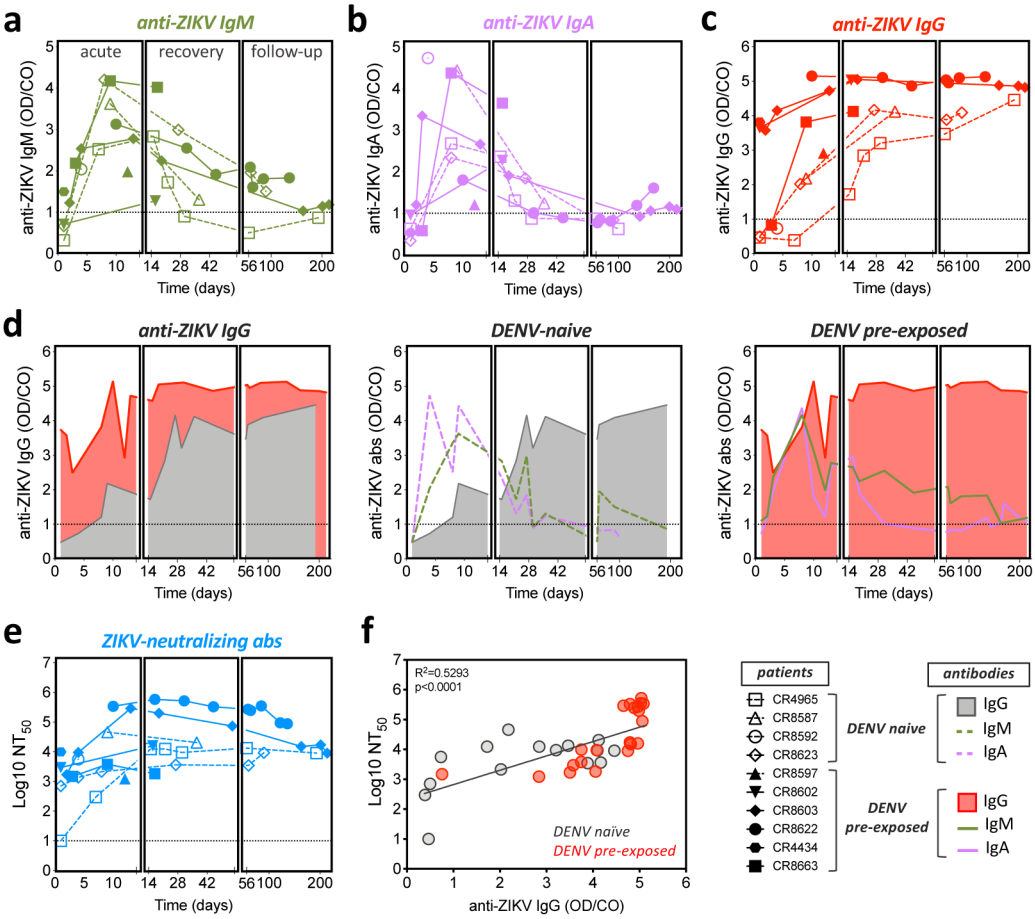

Fig. 2: Dynamics of the humoral response to acute ZIKV infection.

Plasma detection of anti-ZIKV IgM (**a**), IgA (**b**) and IgG (**c**) over time, as determined by ELISA (DIACHECK®) in 10 ZIKV acutely-infected patients. Data are expressed as mean values of OD/CO ratios from n=2 independent experiments. (**d**) Median of anti-ZIKV antibody detection signals within DENV-naïve (n=4) and DENV pre-exposed (n=6) patient groups. (**e**) Titration of anti-ZIKV neutralizing antibodies, overtime. Titers were measured by endpoint titration. The data are expressed as mean values of n=2 (patients CR8587, CR8602, CR8663, CR4434, CR8597 and CR8622), n=3 (patients CR4565 and 8603) or n=4 (CR8623) independent experiments. (**f**) A linear regression model was applied to fit the relationship between anti-ZIKV IgG detection signal intensities and ZIKV-neutralizing antibodies according to patient's previous exposure to DENV status (Total: n=36; DENV-naïve: n=15; DENV pre-exposed: n=21). Pearson correlation coefficient *R* and significance *p* (two-sided) values are reported from the linear regression analysis performed with GraphPad Prism software. (**a-e**) Each patient and previous exposure to DENV status, as defined by the positive detection of anti-DENV IgG at symptom onset, is displayed through unique symbols and connecting lines. Gray dashed lines note assay's detection limits. X-axis, (Time (days)) represents the time from onset of symptoms.

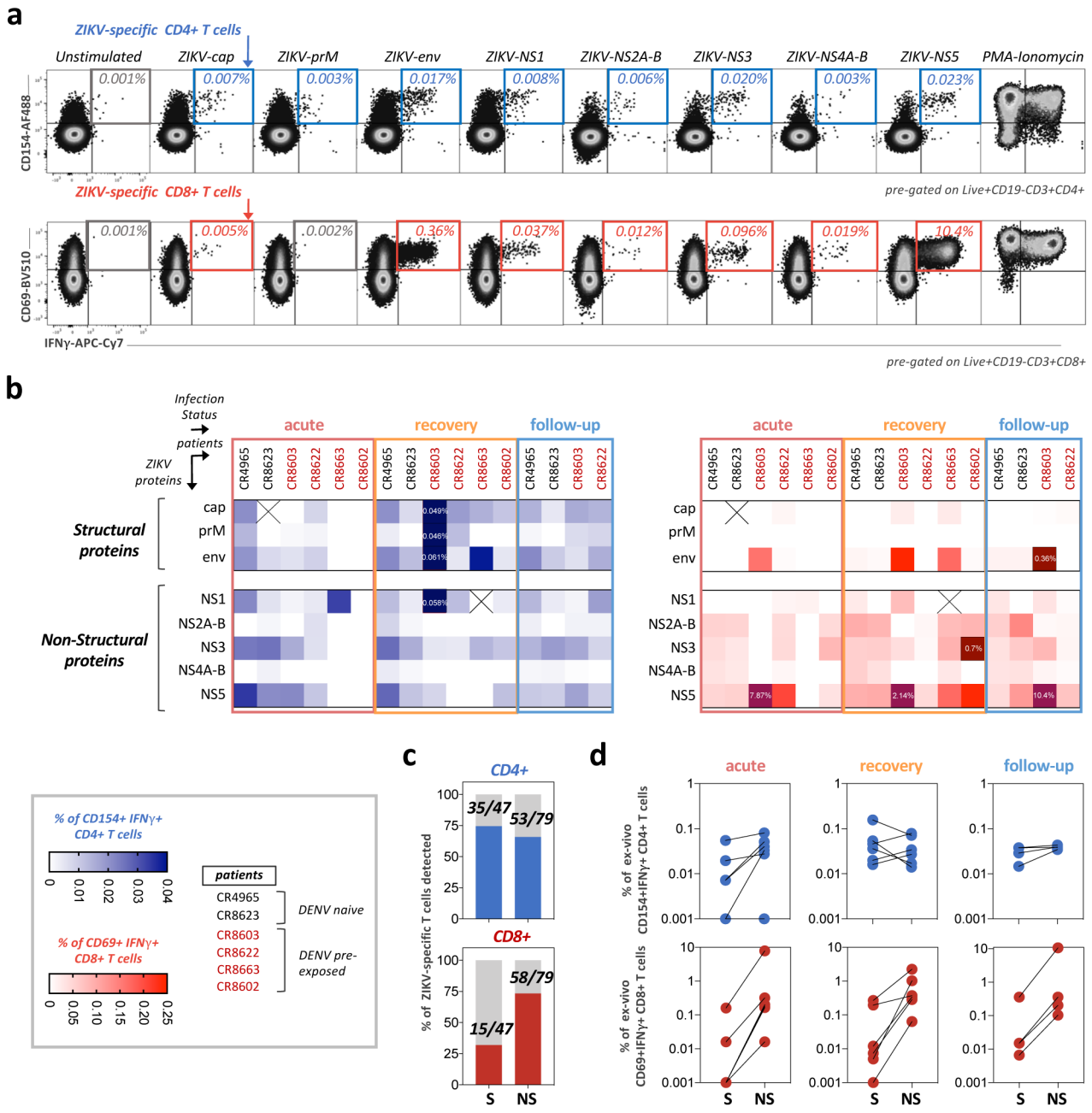

Fig. 3: Dynamics of the cellular immune response to ZIKV infection.

(**a**) Representative flow-plots of intra-cellular cytokine staining (ICS) for the detection of ZIKV-specific CD4+ (upper plots) and CD8+ T cells (lower plots) after stimulation with 15-mer overlapping peptide pools covering the structural as well as non-structural ZIKV proteins. Frequencies of activated-INF**γ**-producing cells are indicated. A positive ICS was determined by the detection of at least 10 ZIKV-specific T cells and a frequency of ZIKV-specific T cells being at least twice the unstimulated signal. (**b**) Detection of ZIKV-specific CD4+ (blue) and CD8+ (red) T cells over time and across six patients by ICS. Frequencies of activated-INF**γ**-producing cells are depicted through a blue (for CD4+ T cells) or red (for CD8+ T cells) color mapping and are expressed as percentages of total CD4+ or CD8+ T

cells. (**c**) Frequencies of samples with positive detection of activated-INFγ-producing cells among total samples tested by ICS as grouped according to the ZIKV regions targeted; Structural (S) (n=47) or Non-structural (NS) (n=79) ZIKV proteins. (**d**) Cell frequencies of activated-INFγ-producing CD4+ (upper charts) or CD8+ (lower charts) T cells targeting Structural (S) or Non-structural (NS) ZIKV proteins. Each dot plot and line represent a single patient (acute n=6; recovery n=6; follow-up n=4).

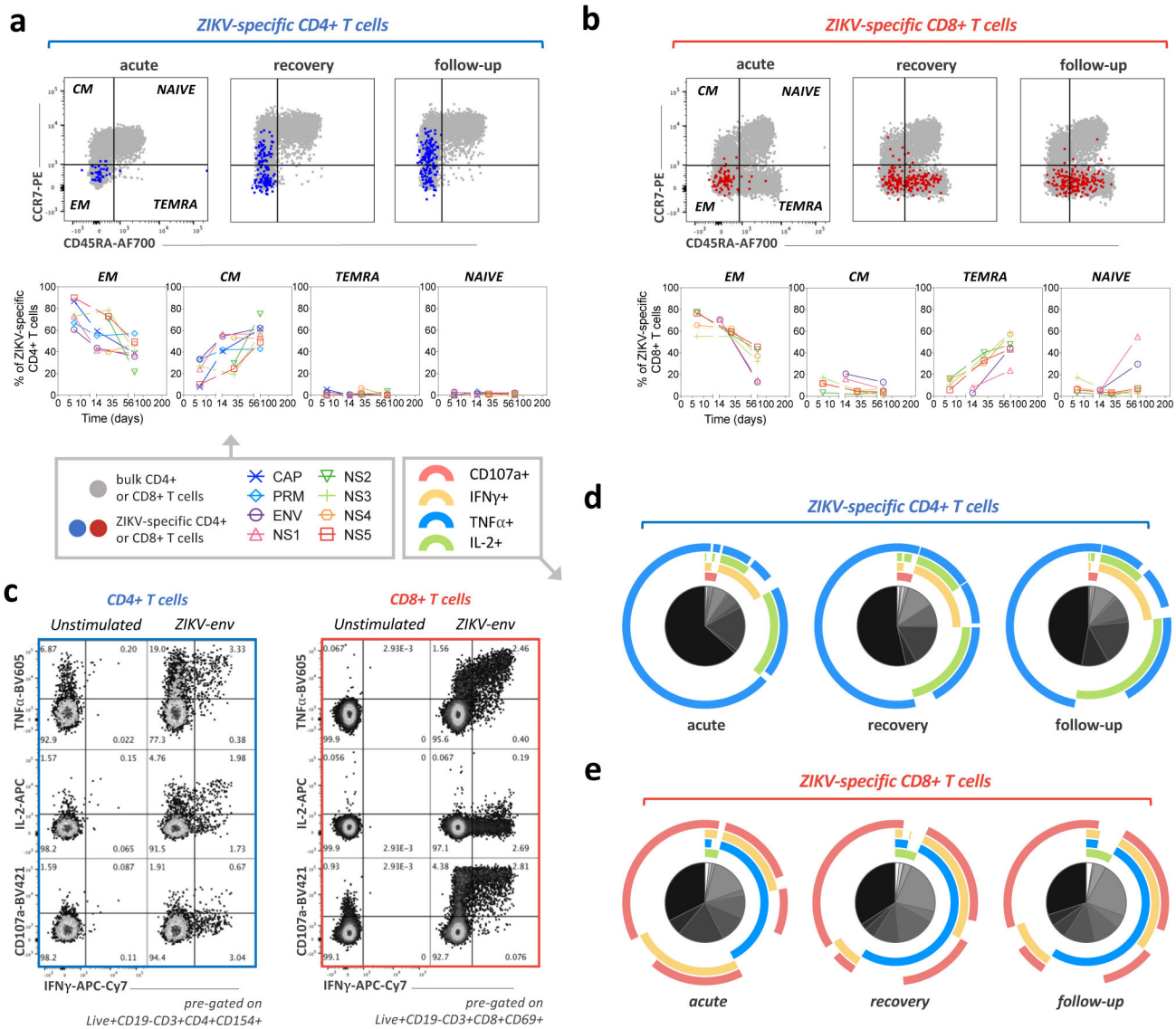

Fig. 4: Memory differentiation and polyfunctionality of ZIKV-specific CD4+ and CD8+ T cells.

T cell memory differentiation based on CCR7 and CD45RA co-expression (naïve: CCR7+CD45RA+; CM: CCR7+CD45RA−; EM: CCR7−CD45RA−; TEMRA: CCR7−CD45RA+). Representative flow-cytometry plots from the analysis of n=6 patients are indicated on the upper charts. Frequencies of ZIKV-specific CD4+ (n=8) (**a**) and CD8+ (n=6) (**b**) T cells across the different memory subsets over time are indicated on the lower charts for patient CR4965. Data from 5 additional patients are displayed in Extended Data Fig. 6. (**c**) Representative flow-cytometry plots, from the analysis of n=4 patients, of cytokine production and cytotoxicity within CD154+CD4+ (left panels) and CD69+CD8+ (right panels) T cells following stimulation with 15-mer overlapping peptide pools. Frequencies of TNFα, IL-2, CD107a and IFNγ-producing cells are indicated. (**d-e**) Overlapping pie charts describing the polyfunctionality of activated CD154+CD4+(**d**) and CD69+CD8+ (**e**) T cells following stimulation with ZIKV-overlapping peptide pools over time. Baseline signals of TNFα, IL-2, CD107a and IFNγ-producing cells in unstimulated

controls have been subtracted from ZIKV-stimulated assays to allow the visualization of ZIKV-specific CD4+ and CD8+ T cell signals. Only time points with detectable CD154+IFNγ+CD4+ (acute n=24, recovery n=26, follow-up n=29) and CD69+IFNγ +CD8+ T cells (acute n=17, recovery n=19, follow-up n=24) from patients CR4965, CR8623, CR8603 and CR8622, as depicted in Fig. 3b, have been used for this analysis. Data represents the median of expression across the different ZIKV-specific T cell responses detected. More detailed representations of the data used in the overlapping pie charts are available in Extended Data Fig. 7.